Electronic Supplementary Material (ESI) for Physical Chemistry Chemical Physics

Hydrogen peroxide electrochemistry on platinum: towards understanding the oxygen reduction reaction mechanism

I. Katsounaros, W.B. Schneider, J.C. Meier, U. Benedikt, P.U. Biedermann, A.A. Auer and K.J.J. Mayrhofer

Supporting information

Thermodynamic considerations

The thermodynamic analysis of H_2O_2 is based on the electrochemical Reactions (1)-(3) and the non-electrochemical bimolecular disproportionation Reaction (4). The corresponding equations for the reaction free energies ΔG and the Nernst equations are summarized in Table S1.

Formally the four electron reduction of oxygen, Reaction (1), corresponds to the sum of the Reactions (2) and (3). Hence, the reaction free energy of (1) is equivalent to the combined reaction free energies $\Delta G_{O_2/H_2O} = \Delta G_{O_2/H_2O_2} + \Delta G_{H_2O_2/H_2O}$, and the standard potential is given by $E^{o}_{O_2/H_2O} = \frac{1}{2} E^{o}_{O_2/H_2O_2} + \frac{1}{2} E^{o}_{H_2O_2/H_2O}$ (using $\Delta G = -nFE$). The disproportionation Reaction (4) can be formally derived as the sum of Reaction (3) and the reversed Reaction (2). Accordingly the reaction free energy is $\Delta G_{2H_2O_2 \leftrightarrows O_2+H_2O} = \Delta G_{H_2O_2/H_2O} - \Delta G_{O_2/H_2O_2}$. Equation (8) defines an equilibrium concentration for H_2O_2 of 0.867×10^{-18} mol l^{-1} at p_{O_2} = 1 atm. At higher concentrations H_2O_2 is unstable with respect to disproportionation into oxygen and water.

Table S1: Reactions, Gibbs free energies and Nernst equations

Reaction	Gibbs free energy	Nernst equation
$O_2 + 4e^- + 4H^+ \rightleftarrows 2\ H_2O$ (1)	$\Delta G_{O_2/H_2O} = \Delta G^{o}_{O_2/H_2O} + RT\ln\frac{\alpha^2_{H_2O}}{\alpha_{O_2}\alpha^4_{H^+}}$ $(\Delta G^{o}_{O_2/H_2O} = -4FE^{o}_{O_2/H_2O} = -2FE^{o}_{O_2/H_2O_2} - 2FE^{o}_{H_2O_2/H_2O_2}$ $= -474.3\ \text{kJ mol}^{-1})$	$E_{O_2/H_2O} = E^{o}_{O_2/H_2O} - \frac{RT}{4F}\ln\frac{\alpha^2_{H_2O}}{\alpha_{O_2}\alpha^4_{H^+}}$ (7) $(E^{o}_{O_2/H_2O} = +1.229\ \text{V})^1$
$O_2 + 2\ e^- + 2\ H^+ \rightleftarrows H_2O_2$ (2)	$\Delta G_{O_2/H_2O_2} = \Delta G^{o}_{O_2/H_2O_2} + RT\ln\frac{\alpha_{H_2O_2}}{\alpha_{O_2}\alpha^2_{H^+}}$ $(\Delta G^{o}_{O_2/H_2O_2} = -2FE^{o}_{O_2/H_2O_2} = -134.1\ \text{kJ mol}^{-1})$	$E_{O_2/H_2O_2} = E^{o}_{O_2/H_2O_2} - \frac{RT}{2F}\ln\frac{\alpha_{H_2O_2}}{\alpha_{O_2}\alpha^2_{H^+}}$ (5) $(E^{o}_{O_2/H_2O_2} = +0.695\ \text{V})^1$
$H_2O_2 + 2e^- + 2H^+ \rightleftarrows 2\ H_2O$ (3)	$\Delta G_{H_2O_2/H_2O} = \Delta G^{o}_{H_2O_2/H_2O} + RT\ln\frac{\alpha^2_{H_2O}}{\alpha_{H_2O_2}\alpha^2_{H^+}}$ $(\Delta G^{o}_{H_2O_2/H_2O} = -2FE^{o}_{H_2O_2/H_2O} = -340.2\ \text{kJ mol}^{-1})$	$E_{H_2O_2/H_2O} = E^{o}_{H_2O_2/H_2O} - \frac{RT}{2F}\ln\frac{\alpha^2_{H_2O}}{\alpha_{H_2O_2}\alpha^2_{H^+}}$ (6) $(E^{o}_{H_2O_2/H_2O} +1.763\ \text{V})^1$
$2\ H_2O_2 \rightleftarrows O_2 + 2\ H_2O$ (4)	$\Delta G_{2H_2O_2 \leftrightarrows O_2 + H_2O} = \Delta G^{o}_{2H_2O_2 \leftrightarrows O_2 + H_2O} + RT\cdot\ln\frac{\alpha_{O_2}\alpha^2_{H_2O}}{\alpha^2_{H_2O_2}}$ (8) $\Delta G^{o}_{2H_2O_2 \leftrightarrows O_2+H_2O} = \Delta G^{o}_{H_2O_2/H_2O} - \Delta G^{o}_{O_2/H_2O_2} = -206.1\ \text{kJ mol}^{-1})$	

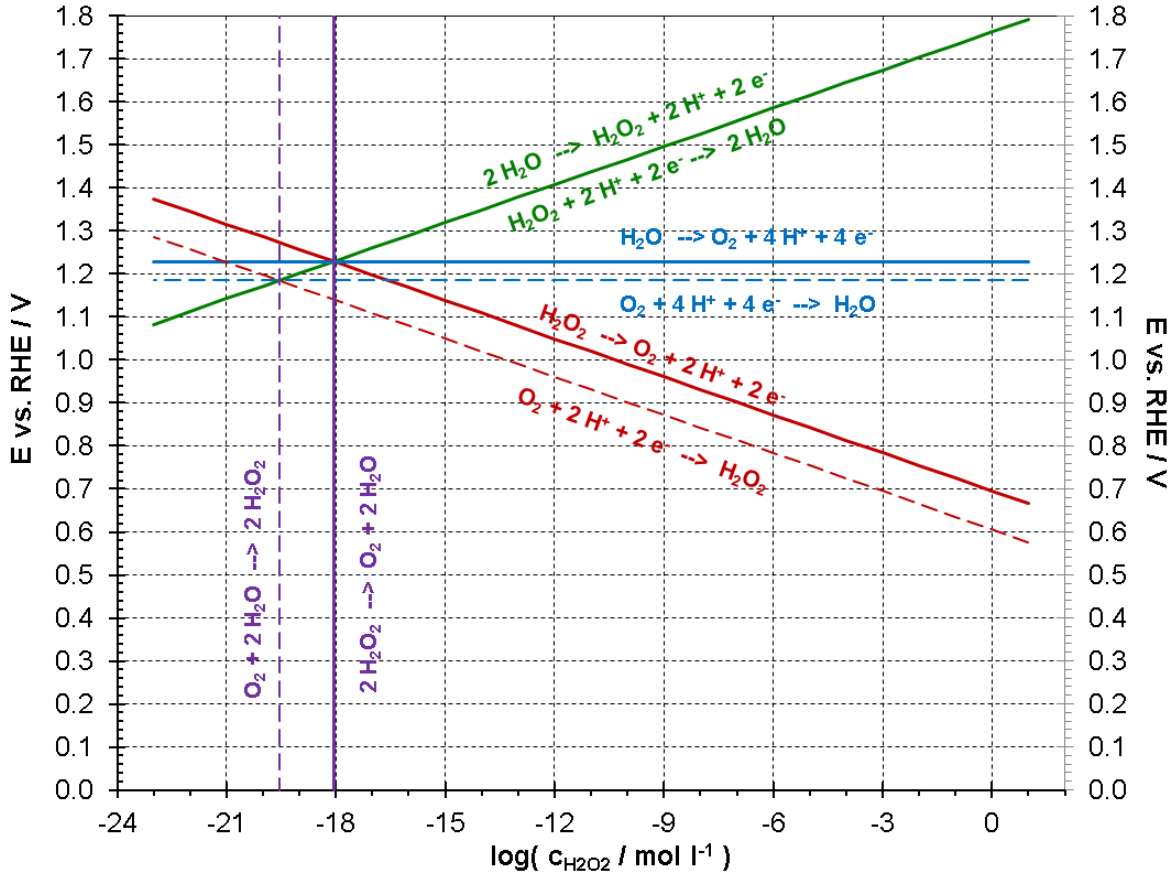

Figure S1. Equilibrium potentials for hydrogen peroxide oxidation (red), and reduction (green) as a function of H_2O_2 concentration at 1 atm O_2. For comparison, the equilibrium potential for direct oxygen reduction (blue) and the equilibrium concentration for non-electrochemical H_2O_2 formation/decomposition (purple) are also shown. Equilibrium lines at an oxygen pressure of 0.001 atm are dashed.

The equilibrium potentials for the PROR as function of the H_2O_2 concentration are shown in Figure S1. The potentials are expressed with respect to the reversible hydrogen electrode (RHE) potential. The diagram is calculated for pH values < 11, where H_2O_2 is undissociated (pKa = 11.63)[2] and an oxygen partial pressure of 1 bar. The effect of the oxygen pressure is indicated by dashed lines, which correspond to p_{O_2} = 0.001 bar.

The equilibrium lines of all four Reactions (1)-(4) intersect in one point because the reactions are formally interrelated (see above). The intersection point corresponds to a state where the thermodynamic driving force for all reactions vanishes.

The Nernst potential for the four electron reduction of oxygen to water is independent of the H_2O_2 concentration and hence appears as a horizontal line in Figure

S1. It separates the regions of oxygen reduction at potentials below +1.229 V_{RHE} (at p_{O_2} = 1 atm) from the regions of oxygen evolution above the equilibrium potential.

Figure S1 shows that at potentials where the oxygen reduction proceeds (<0.9 V), significant amounts of hydrogen peroxide (>10^{-7} mol l^{-1}) may be formed by Reaction (2). Furthermore, the driving force for reduction of H_2O_2 is high. Hence the thermodynamic analysis shows that under these conditions the oxygen reduction may proceed by the "peroxo"-mechanism via a short-lived intermediate H_2O_2.

If H_2O_2 is added to the electrolyte with concentrations >10^{-18} mol l^{-1} it is meta-stable. At potentials between the equilibrium lines for peroxide reduction (Equation (6)) and peroxide oxidation (Equation (5)), reduction as well as oxidation of H_2O_2 are thermodynamically favorable. At lower potentials (below the red line in Figure S1), only the reduction of H_2O_2 has a strong thermodynamic driving force.

In summary, H_2O_2 is stable only at very low concentrations and may be produced in significant amounts either at relatively high potentials by oxidation of water, or at low potentials by reduction of oxygen, provided decomposition reactions are kinetically hindered. At intermediate potentials (around 1.2 V) and concentrations > 10^{-18} mol l^{-1}, H_2O_2 is unstable with respect to oxidation to oxygen, reduction to water and disproportionation.

Cyclic voltammetry at different hydrogen peroxide concentration

The PROR was studied in different H_2O_2 concentrations in the region 1-20x10^{-3} M in a 0.1 M $HClO_4$ supporting electrolyte. The background-corrected cyclic voltammograms (not depicted) scale with the concentration of H_2O_2 in the whole potential region under study; as a consequence, the plots of the dimensionless currents vs. the potential (i/i_L vs. E) coincide for all concentrations (see Fig. S2), as it is expected for diffusion limited processes. Minor differences that are observed in the transition region, particularly close to the diffusion-limited currents, are attributed to uncompensated resistance which was less than 2 Ω. Note that the measured current in this region for the highest concentration is in the order of 10 mA.

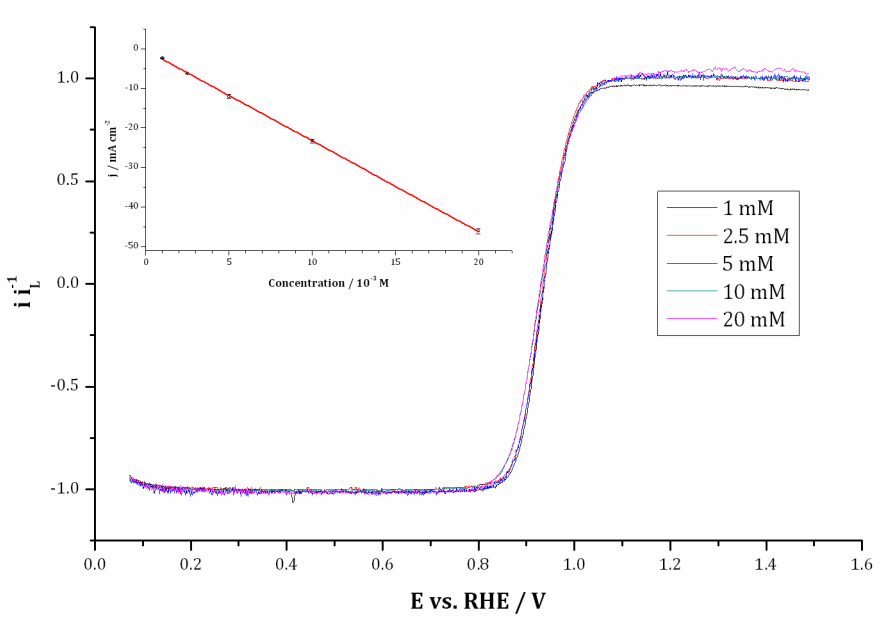

Figure S2. Dimensionless currents vs. the potential (i/i_L vs. E) (positive scan) in different concentrations of H_2O_2 (in the region between $1x10^{-3}$ M and $20x10^{-3}$ M H_2O_2). The inset shows the diffusion-limited reduction current vs. the bulk concentration of hydrogen peroxide. Supporting electrolyte: 0.1 M $HClO_4$. Rotation rate: 1600 rpm. Scan rate: 0.1 V s^{-1}.

The diffusion–limited current for both the oxidation and the reduction of H_2O_2 depends linearly on its concentration, as it is expected from the Levich equation. Using this equation and the slope of the diagram of $i_{L,c}$ vs. concentration (see inset in Fig. S2), the diffusion coefficient of H_2O_2 in 0.1 M $HClO_4$ was calculated as $1.8x10^{-5}$ cm^2 s^{-1}.

Electrolysis experiments

The electrolysis experiments were performed using the following methodology, which is schematically depicted in Scheme S1:

i) First, the electrode was polarized for two minutes at the appropriate potential, while it was rotated with a rate of 2500 rpm.

ii) Then, three cyclic voltammograms were recorded between +0.3 and +1.7 V_{RHE} with a scan rate of 0.2 V s^{-1}, whereas the rotation rate was 400 rpm.

iii) The first step was repeated again.

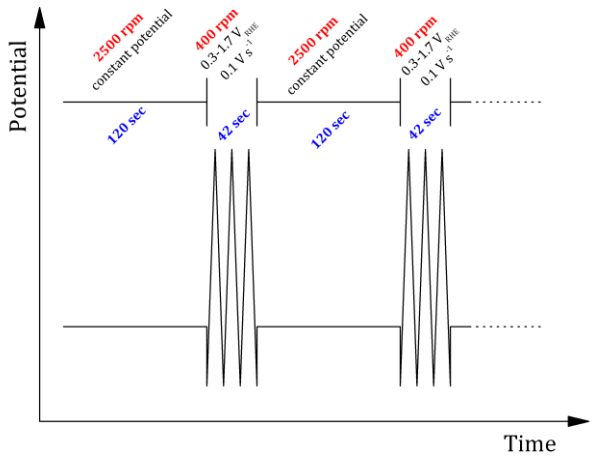

Scheme S1. Methodology for the electrolysis experiments

The cyclic voltammograms in between the constant–potential steps were performed for two reasons: (i) the surface was cleaned because accumulation of impurities (especially at the low potentials) takes place rapidly due to the high rotation rate and (ii) the concentration of H_2O_2 could be directly determined by the diffusion–limited current for the oxidation of H_2O_2 during the positive sweep in the 3rd cycle. The switching of the rotation rate from 2500 rpm (in the constant–potential step) to 400 rpm (in the sweeping experiment) was necessary in order to minimize the contribution of the latter (which lasts in total 42 s for 3 cycles) to the depletion of H_2O_2, nevertheless still being able to determine the concentration of hydrogen peroxide from the diffusion-limited current.

It should be noted that for the calculation of the expected concentration vs. time using Levich and Faraday equations, the rate of decomposition of H_2O_2 during both steps of the experiment (constant potential and potential sweep) was taken into account, considering the time needed in the two different steps and that two different rotation rates were applied. Moreover, the diffusion coefficient that we determined from cyclic voltammetry ($D = 1.8 \cdot 10^{-5}$ cm^2 s^{-1}) was used instead of any literature value.

In the additional experiment at open circuit as mentioned in the text, the current was controlled at zero 2 minutes instead of holding a constant potential; all other conditions of the experiment were the same.

Experiment at open circuit in 0.1 M $HClO_4$ + $20 \cdot 10^{-3}$ M H_2O_2 electrolyte

Figure S3 shows the concentration of hydrogen peroxide vs. time in the experiment at open circuit that was performed in a 0.1 M $HClO_4$ + $20 \cdot 10^{-3}$ M H_2O_2 electrolyte. The comparison with the solid line, which represents the expected concentration decay if the reaction rate is diffusion limited, shows that this is true even in this high concentration of peroxide. The way this experiment was performed, was the same as described above. If the concentration decay is expressed in terms of dimensionless concentration (C(t)/C(0) vs. time, where C(t) is the concentration at time t and C(0) the initial concentration of hydrogen peroxide), then all concentration profiles coincide, regardless of the applied potential or the initial concentration of H_2O_2. This reveals that the rate of decomposition is linearly proportional to the bulk H_2O_2 concentration, which is characteristic for a diffusion-controlled process.

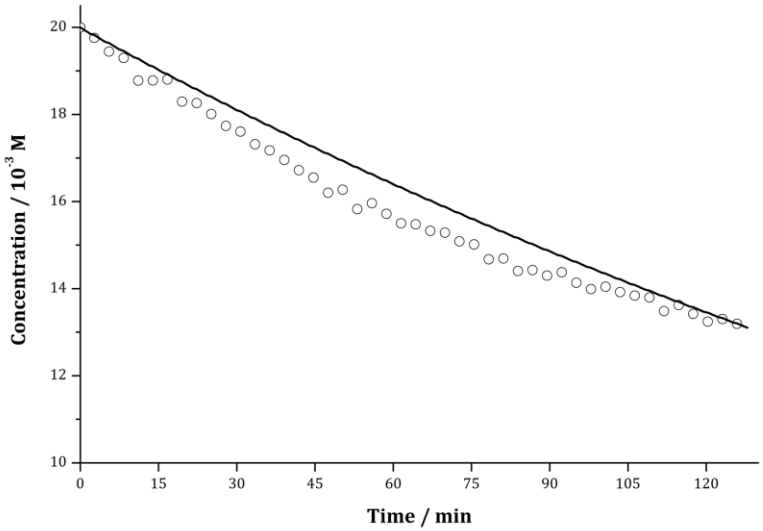

Figure S3. Concentration of H_2O_2 vs. time during the experiment at open circuit in 0.1 M $HClO_4$ + $20 \cdot 10^{-3}$ M H_2O_2. The solid line represents the expected concentration decay for a diffusion–limited reaction rate, using Levich and Faraday equations as described in the paper.

Cyclic voltammetry at different rotation rates

Figure S4 shows the background-corrected cyclic voltammograms in 0.1 M $HClO_4$ + $1 \cdot 10^{-3}$ M H_2O_2 solution at different rotation rates of the platinum working electrode. The data used here are the same as those shown in Fig. 3(c). The current is proportional to the square root of the rotation rate in the whole potential region, even in the transition region. This indicates that the shape of the cyclic voltammogram does not

change with the change of the diffusion layer thickness. In the inset of Fig. S4, the cyclic voltammograms for each rotation rate are normalized to the corresponding diffusion-limited oxidation current, where one can see that the dimensionless cyclic voltammograms coincide for all rotation rates.

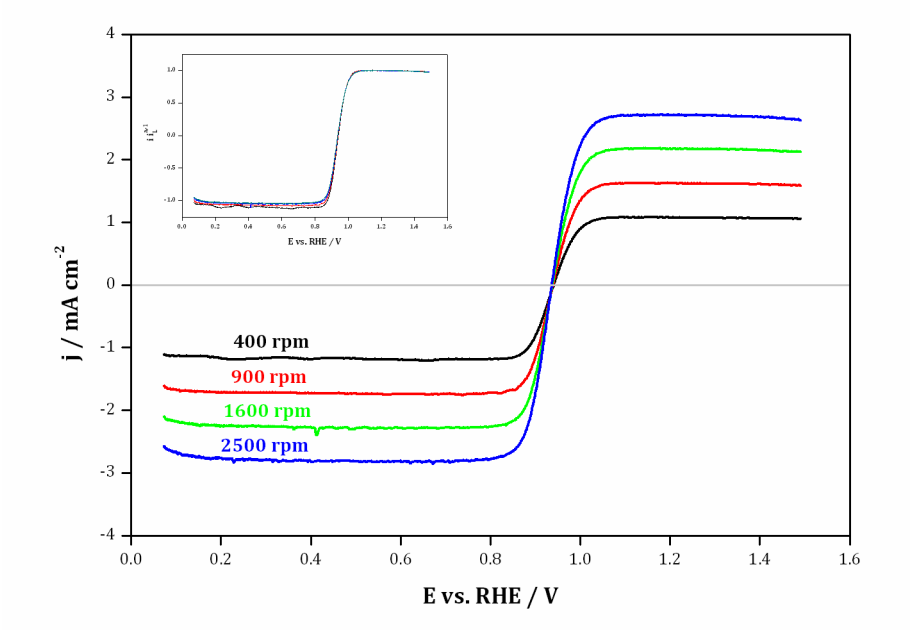

Figure S4. Cyclic voltammograms at different rotation rates in 0.1 M $HClO_4$ + $1 \cdot 10^{-3}$ M H_2O_2. The inset shows the cyclic voltammograms for each rotation rate normalized to the corresponding diffusion-limited oxidation current.

References

(1) Hoare, J. P. In *Standard potentials in aqueous solution;* Bard, A. J.; Parsons, R.; Jordan, J. Ed.; Marcel Dekker: New York, 1985; p. 49.

(2) Pourbaix, M. *Atlas of electrochemical equilibria in aqueous solutions*; Pergamon Press: Brussels, 1966; p. 99.